25th ABCM International Congress of Mechanical Engineering
October 20-25, 2019, Uberlândia, MG, Brazil

COB-2019-0468
EXPERIMENTAL STUDY OF SOOT VOLUME FRACTION AND TEMPERATURE OF LAMINAR NON-PREMIXED ETHYLENE-AIR FLAMES

Ricardo Rabello de Castro
Luís Fernando Figueira da Silva
Pontifícia Universidade Católica do Rio de Janeiro
Department of Mechanical Engineering
R. Marquês de São Vicente, 225 - 22451-900 Gávea, Rio de Janeiro - RJ, Brazil
ricardo_montanha@hotmail.com

Abstract. *Soot particles are combustion derived agglomerates of carbonaceous primary particles that are small enough to stay suspended in the atmosphere. Despite the soot particles role in health and environmental issues, the corresponding formation mechanisms are still poorly known. This work presents measurement results of the soot volume fraction and temperature fields at laminar non-premixed flames. The two-colour pyrometry method is used to obtain the temperature field and the light extinction method the soot volume fraction data. The experiments involved the reconstruction and adaption of a classical non-premixed burner used in previous works. The obtained results are compared to previous works in similar flames exhibiting an agreement that lies within the experimental uncertainty.*

Keywords: *Laminar flame, Laser Extinction, Soot, Two-colour Pyrometry*

1. INTRODUCTION

Soot particles are combustion derived agglomerates of carbonaceous primary particles that are small enough (5 - 30 nm) to stay suspended in the atmosphere. There are multiple reasons to study the soot formation on combustion processes. Included, soot pollution is linked to an increase in cardiovascular disease cases (Bourdel *et al.*, 2017), and to the acidification of lakes and rivers. Futhermore, (Yang, 2018) have found that an increase of 10 μg/m^3 of $PM_{1.0}$ is associated to an increase of 3.2 % of LDL-C and a reduction of 1.4 % of HDL-C, known as "bad cholesterol" and "good cholesterol", respectively. Soot also plays a role in global warming by augmenting the light absorption of snow and ice (Hansen and Nazarenko, 2004). Although this effect is small, compared to those of the usual greenhouse gases, it is still important. Despite the role played in those important health and environmental issues, soot formation pathways are still poorly known and subject of research (Desgroux *et al.*, 2017; Wang, 2011; Garces *et al.*, 2018; Jerez *et al.*, 2019).

In order to understand the soot formation processes, techniques that allow for measurements of soot particle distribution and temperature should be used. Indeed, the reaction rate of a chemical reaction is strongly dependent on local temperature: Arrhenius law states that the reaction rate of a chemical reaction varies with the exponential of the inverse of temperature. Soot particles emit, absorb and scatter radiation on the visible spectrum at typical flame temperatures. Therefore, the spectroscopic analysis of soot radiation allow for the determination of the corresponding distribution (Yan *et al.*, 2017), particle size (Zhao *et al.*, 2014) and temperature (Villanueva *et al.*, 2019). The laser extinction technique (LE) is a non-intrusive optical technique based on the light scattering properties of soot particles (Modest, 2013). Several experimental studies have used the LE technique, but (Zhao and Landommatos, 1998) served as a guide to the present experiments. In this work are described the main optical techniques for soot and temperature measurements. The main advantages of LE are the associated accuracy and simplicity, making it ideal for calibrating more sophisticated techniques, such as Laser-Induced Incandescence (LII).

The two-colour pyrometry technique is also a non-intrusive optical technique that relies on the radiation emission of the soot particles, which provides a two-dimensional mapping of soot temperature. This technique is a simpler, safer and less expensive alternative to techniques such as the Coherent Anti-Stokes Raman Spectroscopy (CARS) which utilizes three laser beams passing through the flame. The technique has been used by (Yan *et al.*, 2017) to reconstruct soot temperature profiles of a ethylene/air flame similar to the one used in this paper.

The objective of this work is to apply the light extinction and two-colour pyrometry techniques to characterize laminar ethylene/air diffusion flame stabilized on a classical standard burner (Gülder and Snelling, 1993). This manuscript is organized as follows: In the first section the experimental methodology will be discussed, following that the soot temperature and soot volume fraction results will be presented and, finally, conclusions will be drawn.

2. EXPERIMENTAL METHODOLOGY

In this section the burner configuration and experiment conditions are presented. Following that, the techniques and experimental setups used to obtain soot distribution and temperature profiles are described.

2.1 Burner setup

The studied Gülder burner is an ethylene/air laminar coflow burner. The dimensions of the burner in this experiment are those laid out by (Gülder *et al.*, 1996) and can be seen on Fig. 1. The flow rate of fuel and oxidizer are controlled by flow meters Alicat Scientific MC-500SCCM-D/5M and Omega FMA5400, respectively. The associated uncertainties at the operating values, specified in Tab. 1, are $\pm$ 15 SLPM for the Omega MFC and $\pm$ 2.55 SCCM for the Alicat MFC. Air flow rate is set to 260 SLPM (4733 cm^3/s) to achieve the same air velocity as (Gülder *et al.*, 1996). Three fuel flow rates have been tested, according to Tab. 1. The first, second and third flow rates correspond to the highest flow rate previously teste in the laboratory, the flow rate specified on Gülder's original work (Gülder *et al.*, 1996) and the flow rate where soot-wings are clearly visible. The flame height has been measured by processing the flame images obtained on the two-colour pyrometry experiment. In this table $\dot{m}_f$, $\dot{m}_o$ are the mass flow rates of ethylene and air respectively, Φ_{global} is the global equivalence ratio and z_{max} the height of the flame. Further details about this burner may be found elsewhere (Jerez *et al.*, 2019).

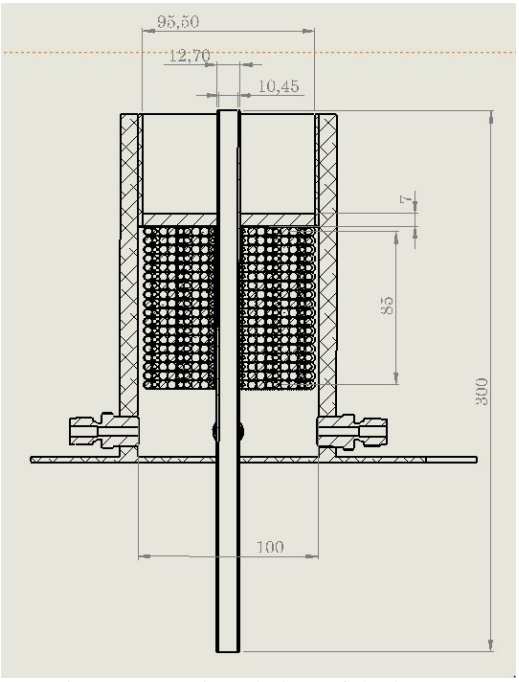

Figure 1: Sectioned view of the burner.

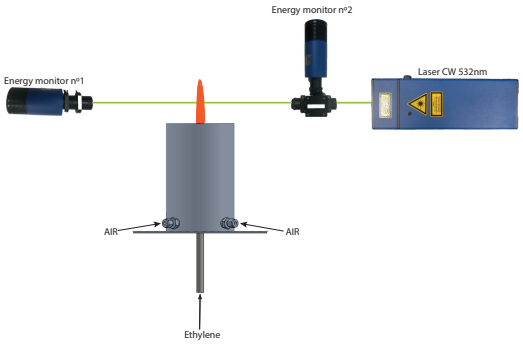

Figure 2: Laser Extinction setup.

Table 1: Experimental flow conditions.

Flow conditions	**Ethylene flow rate (SCCM)**	**Air flow rate (SLPM)**	$\dot{m}_f$ **(g/min)**	$\dot{m}_{ox}$ **(g/min)**	Φ_{global}	z_{max} (mm)
A	100	260	0,12	336	0,0055	31,5
B	194	260	0,24	336	0,0106	62
C	250	260	0,31	336	0,0136	85

2.2 Laser extinction setup

Laser extinction (LE) is used to measure soot volume fraction. The LE technique consists of passing a horizontal laser beam through the flame axis of symmetry measuring the beam intensity before and after the flame, as seen at Fig. 2. The ratio between those intensities can be than used to determine the average value of soot volume fraction along the beam optical path,

$$f_v = \frac{\lambda}{6\pi L \mathrm{Im}\left(\frac{m^2-1}{m^2+2}\right)} \ln\left(\frac{I}{I_0}\right), \tag{1}$$

which allows to determine the soot volume fraction (f_v). The variables m, I, I_0 and L are the complex refractive index, beam intensity after the flame, beam intensity before the flame and optical path length, respectively. The optical path is determined by analyzing a dimensionally calibrated flame image. The complex refractive index ($m = 1,75 \pm 0,61i$) is extracted from (Zhao and Landommatos, 1998) for the corresponding laser wavelength of 532 nm. The LE experimental arrangement has been described in detail by (Jerez *et al.*, 2019).

The experimental procedure consists of adjusting two irises and the gain of the energy monitors in order to have similar intensity readings while the flame is unlit. The resulting beam diameter after calibration is 2 mm. To avoid the interference between with the light emitted by the flame itself a 532 nm band-pass filter is used on the second energy monitor. Additionally, in order to guarantee a stable reading, 100 samples are recorded for each height.

2.3 Two-colour pyrometry setup

The soot temperature distribution is obtained using the two-colour pyrometry technique. This technique relies on the fact that the soot present on the flame is a participating medium that emits, absorbs and scatters light. Provided that the soot natural emission is observed at two wavelengths, λ_1 and λ_2, it is possible to recover the corresponding gray body temperature by means of the Wien approximation of the Planck law (Zhao and Landommatos, 1998):

$$T = \frac{C_2\left(\frac{1}{\lambda_2} - \frac{1}{\lambda_1}\right)}{\ln\left[\frac{J_{\lambda_1}}{J_{\lambda_2}}\left(\frac{\lambda_1}{\lambda_2}\right)^5 \frac{\epsilon_2}{\epsilon_1}\right]}, \tag{2}$$

where λ_i, J_{λ_i}, ϵ_i and C_2 are respectively wavelength (λ_i), monochromatic light intensity, soot emissivity at a specific wavelength and the second Planck constant ($C_2 = 1.438775.10^{-2}\ m.\ K$) . Figure 3 presents the experimental setup employed for the two-colour pyrometry technique. Using a *Imager Intense LaVision* camera and a Nikon NIKKOR lens (f/8 and 1.5 m DOF), a pair of flame images are recorded for each fuel flow rate. A 650 nm band-pass filter is used for the first image and a 850 nm for the second image. These filters have a transmittance of 0.85 and FWMH of 10 nm. An average is taken of 100 flame images on each wavelength.

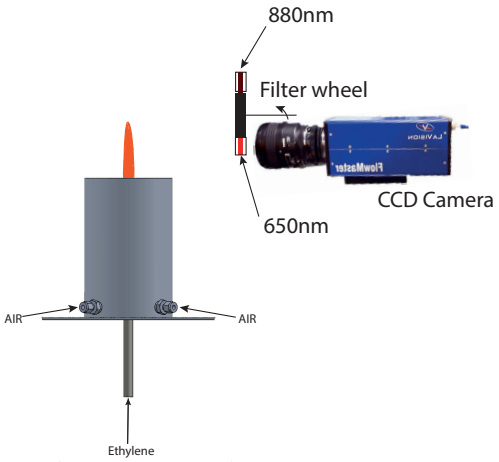

Figure 3: Two-colour Pyrometry setup.

As discussed in previous works (Jerez *et al.*, 2019), the experimental images are line-of-sight integrated, which requires a deconvolution procedure to obtain radial temperature distributions. A Matlab code, adapted from (Cruz, 2017), is used to process the images obtained with the camera. The algorithm is responsible for the deconvolution of the flame images and the determination of the soot temperature field from the two deconvoluted images.

Since the original code yielded non-zero temperatures in regions of the flame where soot is absent, an improvement to circumvent this limitation has been introduced here. These incorrect results came from the fact that the recorded intensities dropped sharply at the base of the flame but, since the temperature is determined based on the ratio between the intensities of each colour [Eq. (2)], the result becomes noisy and incorrect. The solution has been to eliminate the flame regions where the product of those two intensities, J_{λ_1} and J_{λ_2}, is smaller than a arbitrary threshold. This threshold is tuned until the noisy area disappears without affecting the rest of the flame. The used value here is 30% of the average value of the product $J_{\lambda_1}.J_{\lambda_2}$.

2.4 Soot volume fraction and soot temperature uncertainties determination procedure

Several factors have an influence on the LE measurement of soot volume fraction.The equation that defines the relative uncertainty (Taylor, 1996) of f_v is ,

$$\frac{\partial f_v}{f_v} = \left[\left(\frac{\partial \tau}{\tau} \right)^2 + \left(\frac{\partial \lambda}{\lambda} \right)^2 + \left(\frac{\partial E(m)}{E(m)} \right)^2 + \left(\frac{\partial L}{L} \right)^2 \right]^{1/2}. \tag{3}$$

A uncertainty sensitivity evaluation has been conducted by (Cruz, 2017) and the conclusion drawn by the author was that the main uncertainty stems from the refraction index. On the present case the non-dimensionalized uncertainty associated with the refractive index, wavelength (λ), transmissivity and optical path length (L) have been determined to be 16.5%, 0%, 1.4% and 0.7% respectively. Adding to that the type B uncertainty from the transitivity data standard deviation it is possible to write,

$$\frac{\partial f_v}{f_v} = \left\{ \left[\frac{\partial E(m)}{E(m)} \right]^2 + \left[\frac{\partial (\frac{I}{I_0})}{(\frac{I}{I_0})} \right]^2 \right\}^{1/2}, \tag{4}$$

for each measurement point, Where,

$$E(m) = \frac{m^2 - 1}{m^2 + 2} \tag{5}$$

Soot Temperature uncertainty depends on the wavelengths λ_1 and λ_2 and the ratio $R = J_{\lambda_1}/J_{\lambda_1}$. The uncertainties associated with the Planck constant and soot emissivity are not considered here. The temperature associated uncertainty is (Cruz, 2017),

$$\delta T = \left[\left(\frac{\partial T}{\partial \lambda_1} \delta \lambda_1 \right)^2 + \left(\frac{\partial T}{\partial \lambda_2} \delta \lambda_2 \right)^2 + \left(\frac{\partial T}{\partial R} \delta R \right)^2 \right]^{\frac{1}{2}}, \tag{6}$$

where $\frac{\partial T}{\partial \lambda_1}$, $\frac{\partial T}{\partial \lambda_2}$ and $\frac{\partial T}{\partial R}$ can be determined as,

$$\frac{\partial T}{\partial \lambda_1} = \frac{T\lambda_2(C_2 - 6\lambda_1 T)}{\lambda_1 C_2(\lambda_1 - \lambda_2)}, \tag{7}$$

$$\frac{\partial T}{\partial \lambda_2} = -\frac{T\lambda_1(C_2 - 6\lambda_2 T)}{\lambda_2 C_2(\lambda_1 - \lambda_2)}, \tag{8}$$

$$\frac{\partial T}{\partial R} = \frac{T^2 \lambda_1 \lambda_2}{R\lambda_2 C_2(\lambda_1 - \lambda_2)}. \tag{9}$$

These equations indicate that all the sensitivity coefficients are strongly influenced by the inverse of the spectral separation $\lambda_1 - \lambda_2$, which is 230 nm this work. The absolute uncertainties $\delta\lambda_1$ and $\delta\lambda_1$ are given by the full width at half maximum (*FWHM*) values of the filters used in the experiment. The uncertainty parameter δR, on the other hand, is determined using the standard deviation. The uncertainties calculated with these procedures will be discussed on the results section.

3. RESULTS AND DISCUSSION

In this section the results of soot temperature and soot volume fraction are presented and discussed.

3.1 Soot volume fraction results

Figure 4 presents the soot volume fraction results for the three fuel flow regimes given in Tab. 1. In this figure the horizontal axis is the vertical coordinate z, non dimensionalized by the corresponding flame height, z_{max}. Soot volume fraction tends to zero on the upper and lower bounds of the flame, monotonically increasing and, then, decreasing after the maximum value is reached.

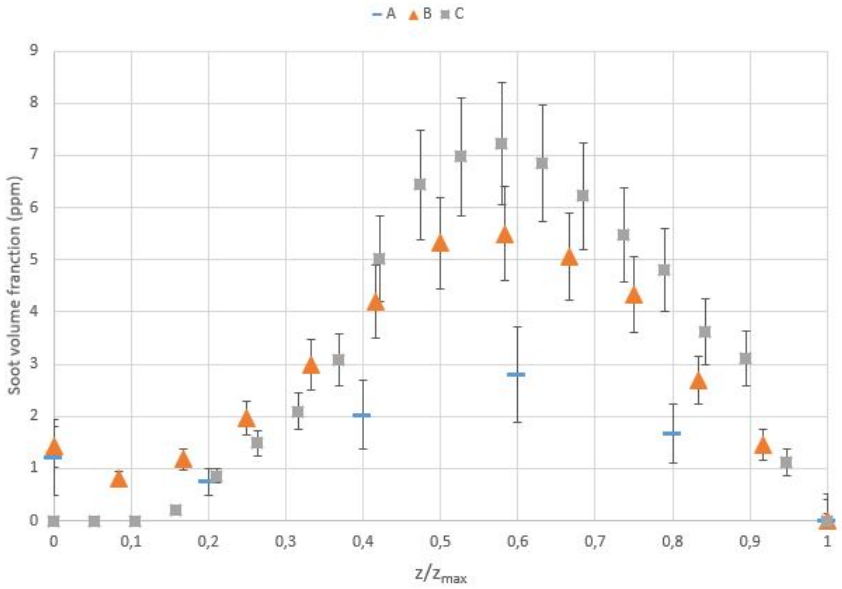

Figure 4: Soot volume fraction measured along the vertical axis for the three flow conditions tested (A, B and C).

A few observations can be made from this Fig. 4:

- Maximum f_v occurs roughly in the same relative height ($z/z_{max} \approx 0,62$) for all studied flames.
- Maximum f_v increases with the fuel flow rate. The maximum values measured were 2.8, 5.6 and 7.2 ppm for flow rates A, B and C respectively.
- Uncertainty is greater on the high f_v regions, reaching over 1 ppm.

At $z/z_{max} = 0.65$ for the regime B, (Cruz, 2017) found $f_v = 6$ ppm, which is within our uncertainty interval (4.7-6.4 ppm). (Gülder and Snelling, 1993) found maximum values of f_v at 7.5 ppm ($z/z_{max} \approx 0.61$) for test conditions similar to regime B. The discrepancy between results could be explained by the beam thickness used (2 mm in this experiment versus 0.3 mm on (Cruz, 2017)), which increase the area where the average soot volume fraction is measured.

3.2 Soot temperature results

Figures 5, 6 and 7 present the soot temperature field on the left, the horizontal temperature profiles for different flame heights (center) and the uncertainty values associated with the measured soot temperature (fields to the right). Note that the vertical scale is different for each figure. Concerning now the soot temperature distributions given on those figures it may be observed that:

- Soot temperatures varies from 1,500 K to 2,100 K.
- As the fuel flow rate increases (A→B→C), high temperature values are found around the lower boundary of the flame.
- In the regime C soot wings may be observed, which indicate that soot is escaping the flame surface without being oxidized.
- Soot temperature drops as fuel flow rate increases(A→B→C), in particular around the flame centerline.

Figure 5 shows that temperature is higher at the outer edge of the flame (around 1,900 K at the edge compared to 1,750 K at the center) and the uncertainty is also higher at this region (reaching over 200 K on some areas).

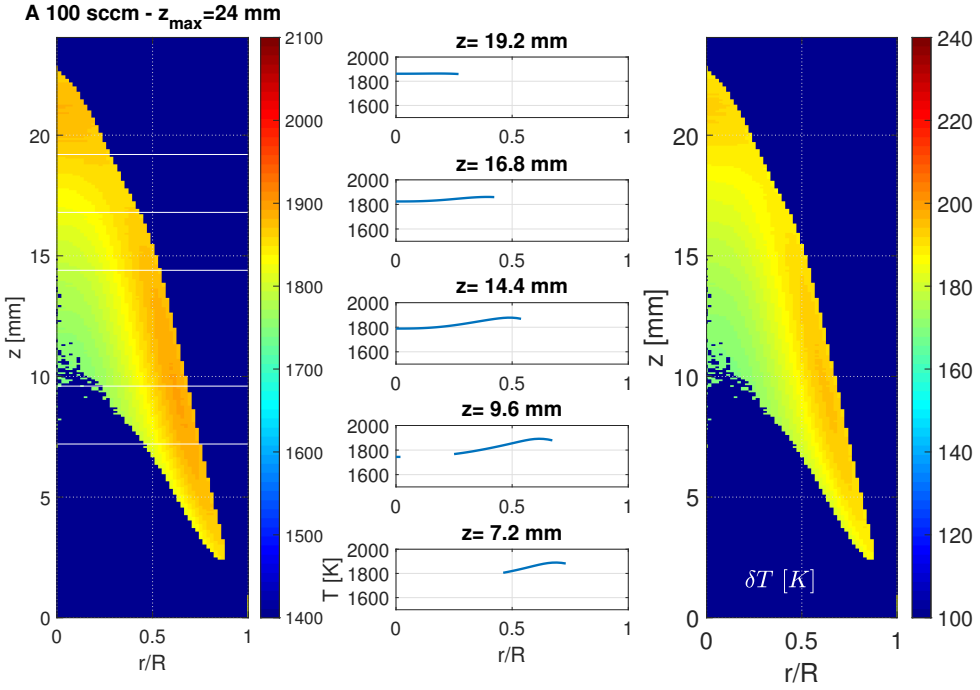

Figure 5: Flow regime A - Soot temperature field (left), horizontal temperature profiles (middle) and temperature uncertainty value (right)

Figure 6 presents lower overall temperatures (1,600-1,850 K) when compared to Fig. 5 (1750-1950 K). Higher temperatures seem to concentrate now at the lower boundary of the flame. Absolute uncertainty values range from 150 K to 190 K.

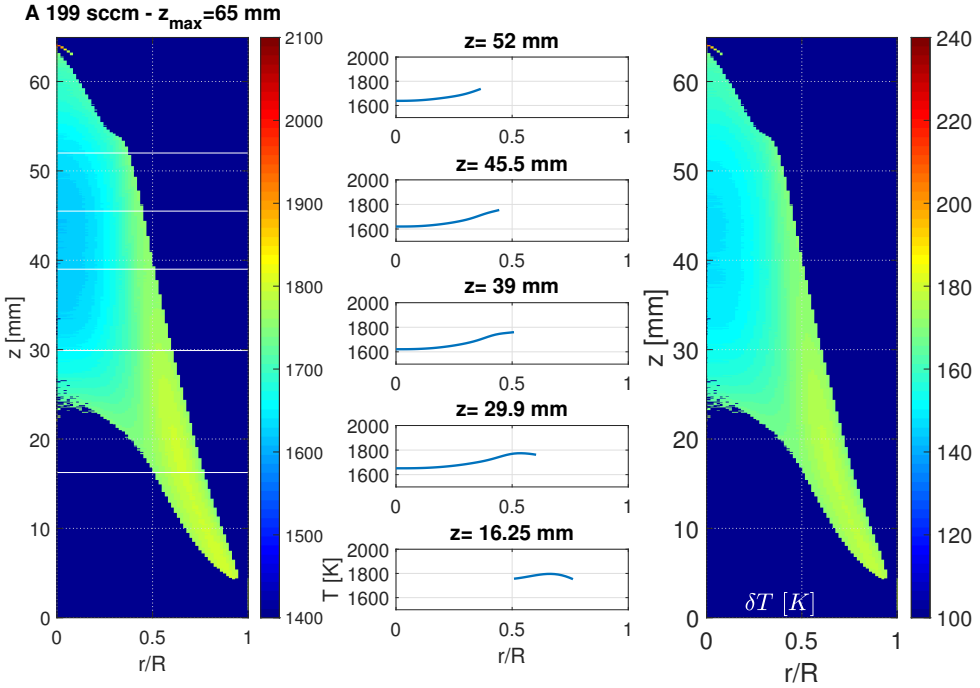

Figure 6: Flow regime B - Soot temperature field (left), horizontal temperature profiles (middle) and temperature uncertainty value (right)

On Fig. 7 soot-wings may be seen at the top of the flame. The concentration of high temperatures at the lower boundary

is clearer and the temperature variation along the horizontal axis is greater. Peak temperatures also seem to be higher when compared to the two previous regimes. The associated uncertainty values range from 140 K to 220 K.

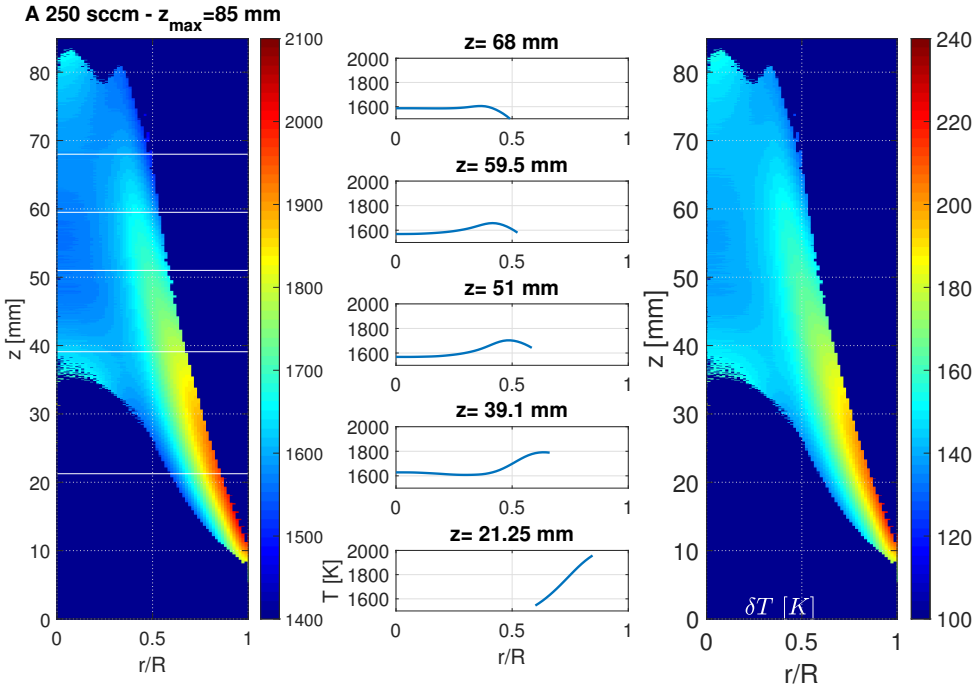

Figure 7: Flow regime A - Soot temperature field (left), horizontal temperature profiles (middle) and temperature uncertainty value (right)

For the regime A the present results may be compared to those of (Jerez *et al.*, 2019), where temperatures ranging from 1,600 to 1,950 K have been measured, which increase monotonically with the height along the centerline of the flame. Here temperatures that varied from 1,750 to 1,880 K, also increasing with height, are observed, but with a small drop at the top of the flame. This last observation is interesting, because it goes against intuition. Previous experimental results found a similar behaviour, and the hypothesis made was that, as soot volume fraction increases with fuel flow rate, the amount of thermal radiation also increases (Jerez *et al.*, 2019). This increase in thermal radiation lowers soot temperature where the soot volume fraction is high.

4. CONCLUSIONS AND PERSPECTIVES

This work has presented soot volume fraction and soot temperature results for three different ethylene flow rates. Both soot volume fraction and soot temperature results were reasonably close to those seen on literature (Cruz, 2017; Jerez *et al.*, 2019). Additionally the results allowed to verify that the smaller air flow rate (60 SLPM) used on previous works in the laboratory (Cruz, 2017) did not affect the results.

Future works on this subject will be devoted to: Study the effect of diluting the ethylene with CO_2 on the soot temperature and especially the volume fraction. Also, PLIF-PAH experiments with higher fuel flow rates (over 100 SCCM) will be performed aiming at unveiling PAH-soot interplay. Finally, it would be interesting to realize PLIF-OH measurements in order to obtain the distribution of OH radical on the oxidizing region of the flame.

5. ACKNOWLEDGEMENTS

This work was performed while L. F. Figueira da Silva was on leave from Institut Pprime (CNRS, France). The authors gratefully acknowledge the support for the present research provided by Conselho Nacional de Desenvolvimento Científico e Tecnológico (CNPq, Brazil) under research grants nos. 306069/2015-6 and 403904/2016-1.

6. REFERENCES

Bourdel, T., Bind, M.A., Bejot, Y., Morel, O. and Argacha, J.F., 2017. "Cardiovascular effects of air pollution". *Archives of Cardiovascular Disease*, Vol. 110, No. 1, pp. 634–642.

Cruz, J.J., 2017. *Estudo Experimental da distribuição de fuligem e de hidrocarbonetos aromáticos policíclicos em chamas laminares não pré-misturadas de etileno e de ar*. Ph.D. thesis, Pontifícia Universidade Católica do Rio de Janeiro, Rio

de Janeiro, Brasil.

Desgroux, P., Faccinetto, A., Mercier, X., Mouton, T., Karkar, D.A. and Bakali, A.E., 2017. "Comparative study of the soot formation process in a "nucleation" and a "sooting" low pressure premixed methane flame". *Combustion and Flame*, Vol. 184, pp. 153–166.

Garces, H., Fuentes, A., Reszka, P. and Carvajal, G., 2018. "Analysis of soot propensity in combustion processes using optical sensors and video magnification". *Sensors*, Vol. 18, p. 1514.

Gülder, O.L. and Snelling, D.R., 1993. "Influence of nitrogen dilution and flame temperature on soot formation in diffusion flames". *Combustion and Flame*, Vol. 92, pp. 115–124.

Gülder, O.L., Snelling, D.R. and Sawchuk, R.A., 1996. "Influence of hydrogen addition to fuel on temperature field and soot formation in diffusion flames". *Twenty-Sixth Symposium (International) on Combustion*, Vol. 26, pp. 2351–2358.

Hansen, J. and Nazarenko, L., 2004. "Soot climate forcing via snow and ice albedos". *Proceedings of the National Academy of Sciences of the United States of America*, Vol. 13, pp. 423–428.

Jerez, A., Villanueva, J.J.C., Figueira da Silva, L.F., Demarco, R. and Fuentes, A., 2019. "Measurements and modeling of PAH soot precursors in coflow ethylene/air laminar diffusion flames". *Fuel*, Vol. 236, pp. 452–460.

Modest, M.F., 2013. *Radiative Heat Transfer*. Academic Press, 3rd edition.

Taylor, J.R., 1996. *Introduction to Error Analysis: The Study of Uncertainties in Physical Measurements*. University Science Books, 2nd edition.

Villanueva, J.J.C., Figueira da Silva, L.F., Cepeda, F. and Fuentes, A., 2019. "Soot pyrometry by emission measurements at different wavelengths in laminar axisymmetric flames". *11th Mediterranean Combustion Symposium*.

Wang, H., 2011. "Formation of nascent soot and other condensed-phase materials in flames". *Proceedings of the Combustion Institute*, Vol. 33, pp. 41–67.

Yan, W., Chen, D., Yang, Z., Yan, E. and Zhao, P., 2017. "Measurement of soot volume fraction and temperature for oxygen-enriched ethylene combustion based on flame image processing". *Energies*, Vol. 10, No. 6, p. 750.

Yang, B., 2018. "Exposure to ambient air pollution and blood lipids in adults: The 33 communities chinese health study". *Environment International*, Vol. 119, pp. 485–492.

Zhao, H. and Landommatos, N., 1998. "Optical diagnostics for soot and temperature measurement in diesel engines". *Progress in Energy and Combustion Science*, Vol. 24, pp. 221–255.

Zhao, H., Williams, B. and Stone, R., 2014. "Measurement of the spatially distributed temperature and soot loadings in a laminar diffusion flame using a cone-beam tomography technique". *Journal of Quantitative Spectroscopy and Radiative Transfer*, Vol. 133, pp. 136–152.

7. RESPONSIBILITY NOTICE

The authors are the only responsible for the printed material included in this paper.